Direct imaging of primary atomisation in the near-nozzle region of diesel sprays

V. Stetsyuk[1]*, C. Crua[1], R. Pearson[2], M. Gold[2]
[1]Centre for Automotive engineering, University of Brighton, UK
[2]BP Global Fuels Technology, Pangbourne, RG8 7QR, UK
*Corresponding author: v.stetsyuk@brighton.ac.uk

Abstract

The spray formation and breakup of n-dodecane was investigated experimentally on a common rail diesel injector using a long working distance microscope. The objectives were to further the fundamental understanding of the processes involved in the initial stage of diesel spray formation under engine-like operating conditions, i.e. high ambient pressure and temperature. Present measurements show that the end of injection is dependent on injection pressure for low injection pressure of 50 MPa and independent for 100-150 MPa pressure range. The end of injection was characterized by large ligaments and deformed droplets along with spherical droplets. It was noted that formation of large droplets during end of injection was not related to injection pressure. The large droplets were found to be in the range of up to 50 μm, which were moving with relatively low velocity. Typical velocity range for large droplets (30-50 μm) was between 1.5 to 5 m/s. The trajectory of individual droplets appeared to be random from injection to injection. It was particularly emphasized that the real fuel injector under engine-like operating conditions can produce a fuel spray, which can be a mix of liquid and vapour at the start of injection.

In this publication we report on progress made with ongoing experimental investigations of the atomisation of n-dodecane by using microscopic imaging and high-speed video using ECN 'Spray A' injector. A long-distance microscopy was used to study near-nozzle region (1.025x0.906 mmm). Our study focuses on the primary atomisation during the start, the steady-state and the end of the injection process.

Introduction

Specific fuel consumption as well as pollutants of current and future diesel engines are directly related to combustion processes. It is expected that a number of vehicles, which use diesel engines will further grow in the future. Despite the fact that current diesel engines have lower specific fuel consumption and higher torque than gasoline engines, NO_x and soot emission may still be a problem [1]. Nitrogen oxide and soot emissions are strongly related to flame temperature and atomisation process [2-8]. The relationship between the combustion process and the spray parameters has been investigated, e.g. by [9-14]. It is quite obvious that fuel atomisation is among of top research priorities due to its direct relationship with pollutants formation.

A detailed characterisation of the near-nozzle region of diesel sprays is necessary in order to fully understand the physics of spray breakup. The modelling of the initial formation of ligaments (partially formed droplets) and subsequent breakup requires experimental data of good quality. At present, experimental characterisation of the initial stage of diesel spray formation is still inadequate, e.g. the distribution of droplets sizes, characterisation of individual droplets at the spray periphery, entire spray statistics etc. There is a number of publications discussing spray formation, liquid breakup processes, the effect of injection pressures on the microscopic spray characteristics etc. [15-34]. The reader is advised to refer to before mentioned publications for further details.

Direct measurements of the droplet sizes under engine-like operating conditions are particularly challenging due to the harsh environment. The most traditional approach relies on high-speed video of an entire spray in order to characterise vapour and liquid penetration. The data, which is obtained during high-speed video measurements, cannot be used for detailed droplets sizing, especially when small droplets are considered. High resolution microscopic imaging seems to be a promising tool in understanding of droplets formation and breakup processes. It becomes an invaluable tool when analysing droplets motion and evaporation of single droplets.

However, there is a number of sources that contribute to the quality of the final post-processed image containing a range of liquid structures. These include motion blurring due to high jet and droplets velocities, optical aberrations and density gradients in an optical chamber. The density gradients in the optical chamber result in refractive index fluctuation, which in turn results in 'motion-blurring type' image distortion.

Recently, the Engine Combustion Network (ECN) an international collaboration among experimental and computational researchers in engine combustion was initiated [35, 36]. The purpose of this collaboration is to provide experimental data, obtained under controlled and standardised operating conditions, as well as to provide a framework for collaborative comparisons of measured and modelled results. The ECN provides a framework for the generation of rigorous experimental data of diesel spray experiments at engine conditions, which can be used for computational spray model development and comparison [35]. The engine operating conditions and the fuel injector were chosen to partially represent the ECN target conditions. It should be noted that the experimental equipment and the operating conditions were not fully compliant with the Spray A target conditions. Therefore, no direct extrapolation of presented results should be done with relation to the ECN conditions.

In this publication we report on progress made with ongoing experimental investigations of the atomisation of n-dodecane by using microscopic imaging and high-speed video during engine-like operating conditions (in-cylinder pressure of 4,8 MPa and temperature of 700K). A long working distance double imaging microscopy was used to study near-nozzle region and track the periphery of the dense spray. Our study focuses on the primary atomisation during the start, the steady-state and the end of the injection process. We present the size, shapes and velocities of liquid structures in the near nozzle region for a range of pressures.

The remaining paper is structured as follows. The next section describes a reciprocating rapid compression machine (RCM), and the optical instrumentation used to study the injection process. The last section describes the results and discusses the findings. The paper ends with a summary of the main conclusions.

Material and methods

A reciprocating rapid compression machine (RCM), based on a Ricardo Proteus research engine, was used in this work. The RCM was a single-cylinder, two-stroke engine 135x150 mm with a displacement of 2.2 litres. The fuel injection equipment consisted of a number of classical common rail components. The high pressure fuel pump was an electrically driven pump connected to a common rail system and is capable of delivering a rail pressure of up to 200 MPa. The injector (number 201.02 ECN Spray A) was a single hole bosh solenoid-activated, generation 2.4, mini-sac, with 0.090 mm nominal nozzle outlet diameter. A low pressure fuel pump was also used to maintain fuel tank temperature constant by providing fuel recirculation through a water-cooled cooling tower. Although, nominal injection pressure was in the range of 50-150 MPa, the actual rail pressure varied due to characteristics of the fuel supply system. The injection pressure was carefully monitored and the difference between the nominal and the actual injection pressure was less than 0.2 MPa.

The illumination sources consisted of a pulsed high-speed monochromatic and incoherent diode laser operating at 690 nm for both the high-speed video and the microscopic imaging. A Phantom V710 high-speed camera was used to characterise the spray vapour penetration and Sensicam CCD camera from PCO was used for the microscopy. The high-speed camera was equipped with 80-200 mm Nikon AF Nikkor lens, which was used at its maximum aperture and zoom. The high-speed videos were recorded at 320 and 400 kfps with a field of view of 7 mm from the nozzle orifice. The nominal spatial scale factors were 32 µm/pixel for high speed video and 0.989 µm/pixel for the long-distance microscopy**.** In-cylinder pressure and temperature were 4.8 MPa and 700K correspondently (corresponding ambient density was 22.8 kg/m^3). The injection pressures were 50, 100 and 150 MPa respectfully. The injection duration based on trigger duration was 1.5 ms for all conditions.

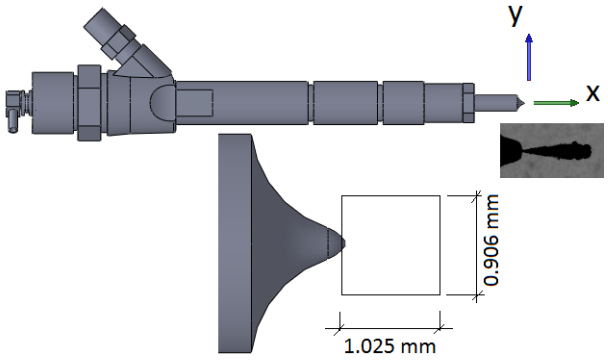

Figure 1: ECN Spray A injector coordinate system used in this work and control volume for microscopic imaging.

Table 1: Specifications for an injector used in this work

Description	Value	Units
Type	Bosh solenoid-activated, generation 2.4	
Nominal nozzle outlet diameter	0.090	mm
Nozzle K factor*	1.5	
Nozzle shaping	Hydro-erosion	mm^3
Mini-sac volume	0.2	
Number of holes	1 (single hole)	
Orifice orientation	Axial (0^0 full included angle)	

* $K = \frac{d_{inlet} - d_{outlet}}{10}$

Table 2: Operating conditions and setup specification

Parameter	Value	Units
In-cylinder pressure (ICP)	48	MPa
Injection pressure	50, 100, 150	MPa
Injection duration (based on trigger)	1.5	ms
Fuel	n-dodecane	-
High speed video scale factor	32	µm/pixel
Microscopy imaging scale factor	0.989	µm/pixel

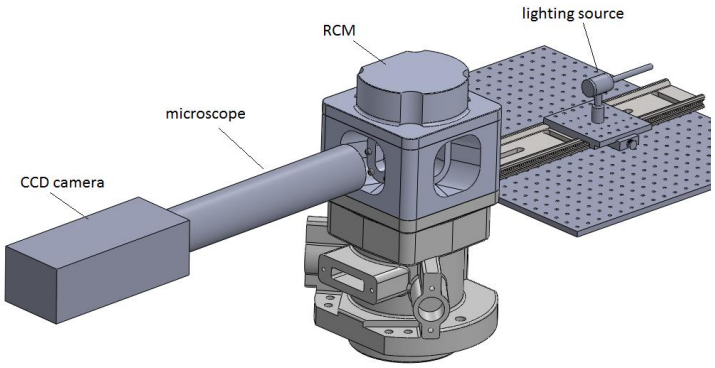

Figure 2: Experimental setup arrangement for microscopic imaging. RCM stands for rapid compression machine. A pulsed high – speed monochromatic and incoherent laser diode with λ=690 nm was used as a lighting source. For high-speed video, the same setup was used except CCD camera.

Results and discussion

Figure 3 shows raw high-speed shadowgraphy images as a function of time after start of injection (ASOI) as well as a comparison of penetration measurements during motored conditions for ICP of 4.8 MPa with Sandia spray A data. We used a set of MATLAB© code for image processing in order to extract vapour jet penetration, which was published by Sandia. The jet vapour-boundary and spreading angle are detected and plotted against time ASOI. We also compared our data obtained from motored conditions with Sandia spray A data. The penetration is shown in Figure 3. Presents measurements slightly overpredict the Sandia data, which can be due to not fully ECN compliant hardware.

Figure 4 shows the liquid-vapour mixture exiting the nozzle hole for 0.295 ms ASOI for ICP of 48 bar and injection pressure of 150 MPa. The most distinctive feature shown in this image is the so-called vapour pre-jet, which issues from the injector orifice prior to liquid jet. The vapour pre-jet is a well-defined axisymmetric mushroom-like vapour jet issuing sub-sonically into hot, still, compressed air. The extent of this vapour pre-jet is circa 180 µm and does not vary from injection-to-injection significantly.

The vapour pre-jet can be caused by one or more of the following: expansion of cavitation pockets after previous injection; ingestion of in-cylinder gases after previous injection; heating and evaporation of fuel trapped inside orifice between injections. Figure 4 also shows fuel jet penetrating through vapour, which emerged prior to liquid. It can be suggested that is this vapour consists of heated and evaporated fuel trapped inside the orifice, which can be ignited by the hot air mixed with remaining burnt products in a cylinder. It also noted that the vapour pre-jet has clearly visible

vortical structures, which can be seen under higher resolution (0.6 µm/pixel). The fuel jet continuous to penetrate the vapour pre-jet, as results, the vapour pre-jet cannot maintain the shape of a mushroom-like structure.

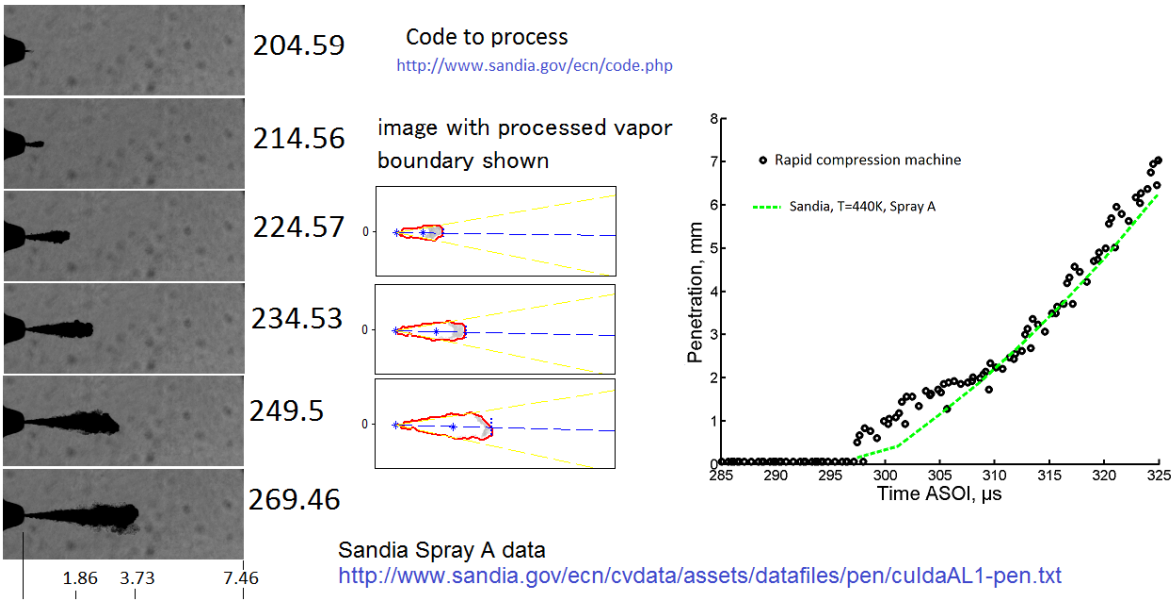

Figure 3: Raw high-speed shadowgraphy images as a function of time ASOI (µm). Note that horizontal scale is mm for ICP of 4.8 MPa. Example of processed images with spray boundary is also shown in red. On the right, penetration measurements during motored conditions for ICP of 4.8 MPa compared with Sandia spray A data.

Droplets can be seen to form at the jet periphery almost the instant the jet exits the nozzle. We observed droplets with typical diameter between 2 and 4 µm at the periphery of the spray during start and steady-state phases of injection. However, at present no detailed data on droplets sizes at the jet periphery is presented here apart from conceptual description.

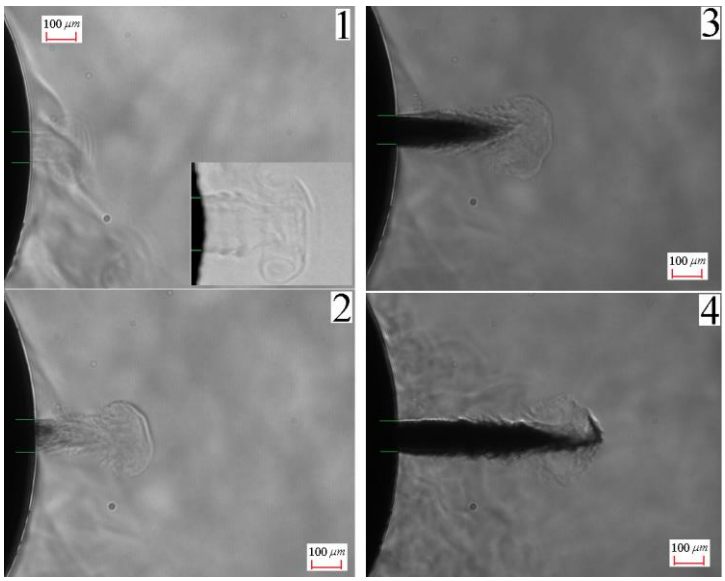

Figure 4: Liquid-vapour mixture exiting the nozzle hole for 0.295 ms after start of injection (ASOI) at injection pressure of 150 MPa. In-cylinder pressure (ICP) was 4.8 MPa. Vapour pre-jet is also shown under greater resolution on top left image. Nozzle position is shown by the two short horizontal lines. Field of view is 1.025 (horizontal) x 0.906 (vertical) mm.

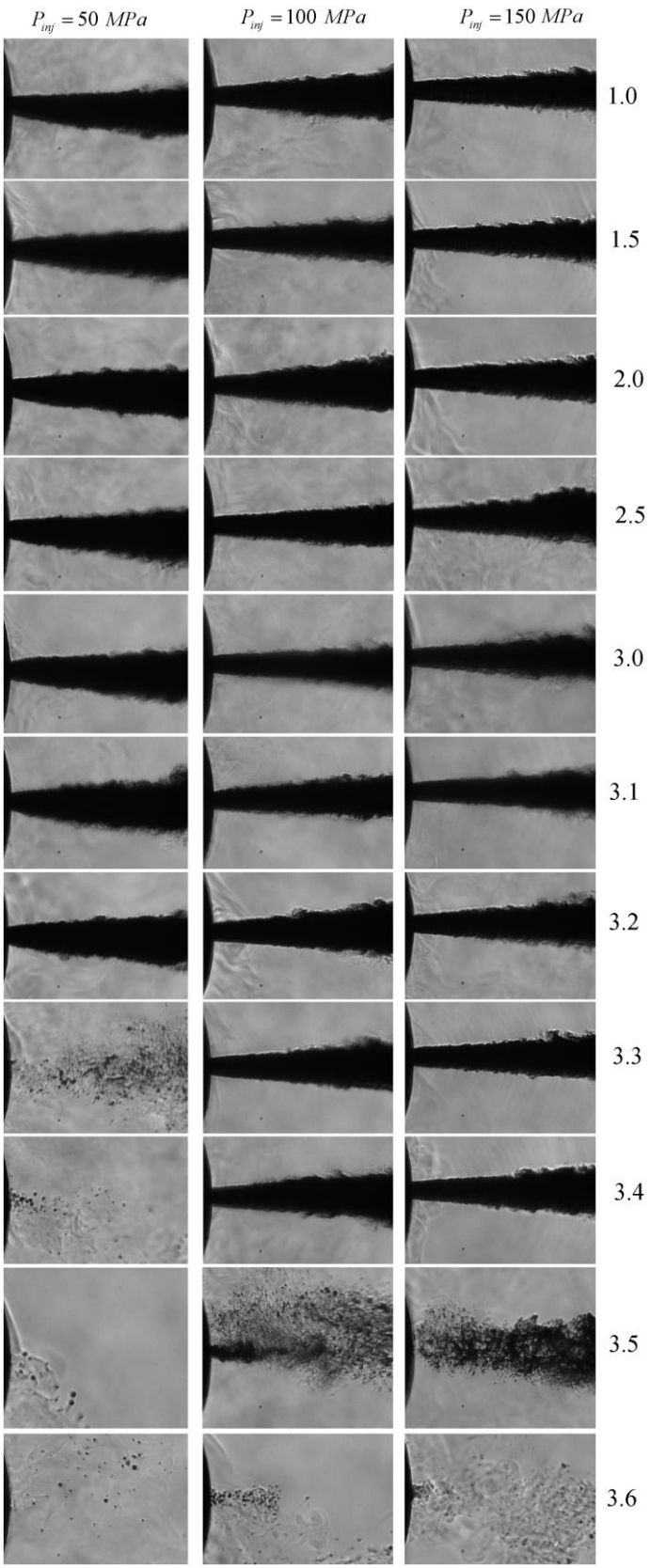

Figure 5: Steady-state and end of injection (EOI) for 50 (left), 100 (middle) and 150 (right) MPa as a function of time ASOI. ICP is 4.8 MPa. All timings are after start of injection (ASOI) command. Each sequence represents field of view of 1.025 (horizontal) x 0.906 (vertical) mm.

Figure 5 shows an image sequence of spray evolution during steady-state period and the end of injection for different injection pressures. Note that the image sequence is built up from individual instantaneous realisations from different injection cycles. It should be emphasised that in order to build up an image sequence in such a way, a highly stable and reproducible injection even is required. In this work it was observed through a series of instantaneous injection realisations that the spray was highly stable and reproducible. It is, therefore, suggested that Figure 5 represents the spray evolution with high degree of accuracy even if individual images are taken from independent injection cycles. On the other hand, it is virtually impossible to capture fast and transient phenomena by using an image sequence. However, the detailed analysis of temporally resolved spray evolution is beyond the scope of the present work.

Figure 5 clearly shows that for low injection pressure of 50 MPa the steady-state injection period is quite long. It is particularity hard to notice when the needle starts closing, i.e. when the end of injection occurs. Nominal trigger duration was 1.5 ms, which would suggest that the end of injection starts at 1.7-1.9 ms after the start of trigger (nominal injection duration+ hydraulic delay). However, according to the present figure the injection process continues until 3.2 ms ASOI. At 3.3 ms ASOI the spray becomes unstable and breaks down into a bunch of small and large droplets. It was also noted that large ligaments and highly deformed droplets were present. Large droplets issuing from the nozzle orifice were observed even at 3.6 ms ASOI, i.e. 2.4 times the nominal injection duration. Intermediate and high pressures, i.e. 100 and 150 MPa demonstrate similar trend as low pressure spray. The steady-state period lasts for circa 3.4 ms ASOI and ends in a similar way as for 50 MPa. However, ligaments are longer than for low pressure sprays and the spray looks denser during the end of injection.

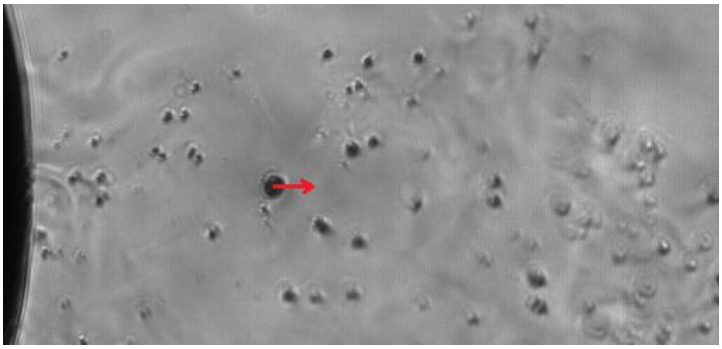

Figure 6: End of injection for injection pressure of 100 MPa and 3.7 ms ASOI. Droplet velocity vector is shown as red line (V_x=5, V_y=0 m/s). Field of view is 1.025 (horizontal) x 0.486 (vertical) mm. Diameter of this droplet is 30 μm.

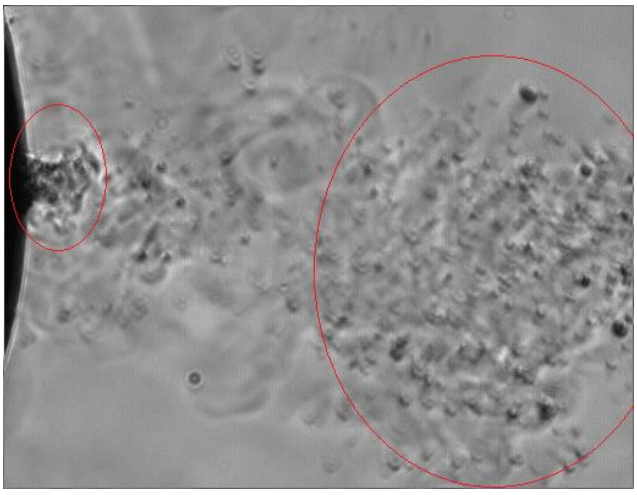

Figure 7: Secondary injection event after the end of injection for injection pressure of 150 MPa for 3.6 ms ASOI. Field of view is 1.025 (horizontal) x 0.779 (vertical) mm. A cloud of droplets from the end of injection is shown on the right as red encircled area. Secondary injection even is shown on the left also as red encircled area.

The end of injection is clearly visible (Figure 5) and can be characterised by unsteady behaviour of the fuel spray. At this stage, the fuel jet consists of individual droplets, which in some cases can be quite large. However, even at this stage, a dense spray can still be observed, which is composed by droplet ensemble of various sizes. The droplet shape during end of injection is often can be approximated by a spheroid for high injection pressures i.e. 100 and 150 MPa. On the other hand, for low pressure sprays, i.e. 500 bar, large ligaments as well as highly deformed droplets are observable. The detailed characterisation of droplet shape as well as three-dimensional reconstruction of measured droplets, in order to accurately predict the droplet surface area and its volume, will be presented in the future paper. It should be emphasized that conventional algorithms for droplet sizing, which are based on computation of a number of pixels within droplet area, can lead to highly biased results, if highly deformed droplets are present in the fuel sprays.

It has been observed that the trajectory of individual droplets during the end of injection can significantly vary from injection to injection. This can be related either to unsteady nature of the injection process at this stage or to the air motion during expansion stroke. Clearly visible vapour trails behind each droplet are a clear sing of evaporation process during droplets travel time.

It should be noted that the fuel jet continues to penetrate the ambient air even after the end of injection. This can be due to the remaining momentum possessed by the collapsing jet resulting in secondary injection event. This even can be seen in Figure 7. The figure shows the end of injection for 3.6 ms ASOI and injection pressure of 150 MPa. Two zones are clearly visible, in which on the right hand side is a cloud of droplets formed after the end of injection. On the left hand side on the same Figure, a zone of droplet ensemble of various sizes is visible. We refer to this zone, as secondary post-injection event. It is still unclear whether this happens due to bouncing of the nozzle needle at the end of injection or due to another reason.

Conclusions

Present papers presented ongoing experimental investigation of the atomisation of n-dodecane by using long working distance microscopic imaging and ECN Spray A injector under engine-like operating conditions. Although it is very difficult to measure the droplet sizes under such harsh operating conditions, especially at the fuel jet periphery and in the vicinity of the nozzle, the laser long-distance microscopy can be a very useful experimental method of investigating primary atomisation and breakup mechanisms. Fluctuations in refractive index in cylinder during motored conditions lead to motion-type blurring images, which have to be discarded if the image quality is not sufficient enough. This requires a large number of images to be acquired in order to obtain reliable statistical data.

It was particularly emphasised that the real fuel injector under engine-like operating conditions produces a fuel spray, which can be a mix of liquid and vapour at the start of injection. Future computational models should be able to capture this phenomenon as it is likely to influence the spray penetration and subsequent combustion. It was suggested that the vapour pre-jet can be a source of potential ignition source due to its presence in the vapour phase and subsequent rapid mixing with hot air leading to spontaneous ignition.

Present measurements show that the time when the end of injection starts to be clearly visible is dependent on the injection pressure for fixed injection duration (fixed trigger duration). Although trigger duration was fixed, low injection pressure, which was relevant to low and idle conditions resulted in a shorter injection duration compared to high pressure sprays. The end of injection characterized by large ligaments and deformed droplets along with spherical droplets. It was noted that formation of large droplets was not related to injection pressure. The large droplets were found to be in the range of up to 50 µm, which were moving with relatively low velocity. Typical velocity range for large droplet (30-50 µm) was between 1.5 to 5 m/s. The trajectory of individual droplets appeared to be random from injection to injection.

Acknowledgement

The authors would like to thank BP Formulated Products Technology and the EPSRC (EP/K020528/1) for financial support. The EPSRC Engineering Instrument Pool is also acknowledged for supplying equipment.

References

[1] Heywood, J. B., 1988, "Internal combustion engine fundamentals."
[2] Lefebvre, A. H., 1982, "Gas Turbine Combustors".
[3] Lefebvre, A. H. 1995, Journal of Engineering for Gas Turbines and Power, 117, pp. 617–655
[4] Kouremenos, D. A. and Hountalas, D.T., 2001, SAE paper 2001-01-0198.
[5] Yang, F. and Minggao, O., 2003, SAE paper 2003-01-0351.

[6] Deepak, A., et al., 2011, Applied Energy, 88, pp. 2900–2907.
[7] Glassman, I., 1988, 22nd Symposium (International) on Combustion, 22, pp. 295–311.
[8] Pickett, L.M. and Siebers, D. L., 2002, Proceedings of the Combustion Institute, 29, pp. 655–662.
[9] Siebers, D. and Higgins, B., 2001, SAE Technical Paper 2001-01-0530.
[10] Higgins, D. and Siebers, D. L., SAE Paper No. 2001-01-0918, 2001.
[11] Yi, Y. and Reitz, R. D., SAE Paper No. 01-1041, 2003.
[12] Choi, C. Y. and Reitz R. D., 2000, Combust. Sci. Technol. 159, pp. 169–198.
[13] Arcoumanis, C. and Gavaises, M., 1998, Atomization Sprays 8, pp. 307–347.
[14] Patterson, M. A. and Reitz R. D., 1998, SAE Technical Paper 980131.
[15] Linne, M. A., et al., 2009, Proceedings of the Combustion Institute 32, pp. 2147–2161.
[16] Linne, M, et al., 2010, Experiments in Fluids, 49(4), pp. 911–923.
[17] Klein-Douwel, R.J.H., et al., 2007, Fuel, 86, pp. 1994–2007.
[18] Delacourta, E., et al., 2005, Fuel, 84, pp. 859–867.
[19] Mohammad, R. H., et al. 2013, Experimental Thermal and Fluid Science 50, pp. 10–20.
[20] Shoba, T. T. et al., 5-7 September 2011, 24th European Conference on Liquid Atomization and Spray Systems, Estoril, Portugal.
[21] Bae, C., et al., 2002, SAE 2002-01-1625.
[22] Badock, C., et al., 1999, International Journal of Heat and Fluid Flow, 20(5), pp. 538–544.
[23] Heimgärtner, C. and A. Leipertz, Pasadena, California, 2000, USA, July 16-20, 8th International Conference on Liquid Atomization and Spray Systems, .
[24] Shoba, T., et al., 5-7 September 2011, 24th European Conference on Liquid Atomization and Spray Systems, Estoril, Portugal,
[25] Sung, W. P, et al., 2006, International Journal of Multiphase Flow 32, pp. 807–822.
[26] Bae, C., et al., 2002, SAE Technical Paper 2002-01-1625.
[27] Heimgärtner, C. and Leipertz A., 2000, SAE 2000-01-1799.
[28] Lai, M.-C., et al., 1998, SAE 982542.
[29] Sjoberg, H., et al., 1996, Optical Engineering, 35(12), pp. 3591-3596.
[30] Crua, C., et al., 2010, SAE 2010-01-2247.
[31] Pickett, L.M., et al., 2011, SAE 2011-01-0686.
[32] Crua, C., et al., September 2-6 2012, 12th International Conference on Liquid Atomization and Spray Systems Heidelberg, Germany.
[33] Manin, J., et al., September 11-14 2012, THIESEL 2012 Conference on Thermo- and Fluid Dynamic Processes in Direct Injection Engines, Valencia, Spain.
[34] Pickett, L.M., et al., 2012, SAE 14PFL-1086.
[35] Engine Combustion Network website http://www.sandia.gov/ecn/ ([cit. 2014-06-22])
[36] Pickett, L.M., et al., 2010, SAE 2010-01-2